A Cold Event in Asia during January–February 2012 and Its Possible Association with Arctic Sea Ice Loss

BINGYI WU

Institute of Atmospheric Sciences, Fudan University, Shanghai, and Chinese Academy of Meteorological Sciences, Beijing, China

KUN YANG

National Meteorological Center, Beijing, China

JENNIFER A. FRANCIS

Department of Marine and Coastal Sciences, Rutgers, The State University of New Jersey, New Brunswick, New Jersey

(Manuscript received 5 February 2016, in final form 22 June 2017)

ABSTRACT

Through both observational analyses and simulation experiments, this study investigates the intraseasonal evolution of atmospheric circulation anomalies associated with a persistent cold event in the Asian continent during late January–early February 2012, and the possible association with Arctic sea ice loss and Arctic atmospheric circulation during the preceding summer. The results suggest that the northeastern Pacific–Aleutian region and central Eurasia are two critical areas where the atmospheric circulation evolution contributed to the development of this cold event. A persistent increase in sea level pressure (SLP) over the Aleutian region was a predominant feature prior to the cold event, and then decreasing SLP over this region was concurrent with both occurrence of a polar blocking high aloft and rapid strengthening of the Siberian high, triggering outbreaks of Arctic air over the Asian continent. Consequently, the influence of the Aleutian region on this cold event (i.e., the downstream effect of the atmospheric circulation) played a critical role. Simulation experiments demonstrate that Arctic atmospheric circulation conditions in the summer of 2011 significantly enhanced a negative feedback of Arctic sea ice loss on atmospheric circulation over the Aleutian region and central Eurasia during the ensuing wintertime, which could have led to the favorable atmospheric circulation that facilitated the occurrence of cold events resembling the one in 2012. This study also implies that the Aleutian low and disturbances in the midlatitudes over the northeastern Pacific may provide precursors that could increase skill in predicting the intraseasonal evolution of extreme cold events over Eurasia.

1. Introduction

During the past decade, Eurasia has suffered frequent cold winters and extreme weather events. For example, Japan experienced extreme snowfalls in December 2005; China suffered rare persistent cold and freezing rain events in January–February 2008; Eurasia was extremely cold during January–February 2012, along with temperatures below the 2nd percentile in Belgrade and Siberia (WMO Regional Climate Centres 2012). According to media reports, more than 700 Europeans died from the extreme cold winter of 2011/12. The recent cold winters and extreme weather events over East Asia were related to the reamplification of the East Asian winter monsoon (Wang and Chen 2014). North America also suffered extreme cold and heavy snowfalls in the two consecutive winters of 2013/14 and 2014/15. In 2013/14 the Great Lakes were almost completely frozen for the first time over the previous 35 years (Van Oldenborgh et al. 2015), and in 2014/15 Boston broke its winter snowfall record, with a total of 2.7 m. These extreme events were covered extensively by the media.

Extreme cold and heavy precipitation events affect not only social and economic activities in the populous region of the world, but they also influence convection patterns in the low latitudes of East Asia, which further induce atmospheric circulation anomalies across a broad region (Chang and Lau 1980, 1982; Ding and Krishnamurti 1987; Ding 1990; Zhang and Wang 1997; Gong and Ho 2002; Takaya and Nakamura 2005a,b;

Corresponding author: Bingyi Wu, bywu@fudan.edu.cn

DOI: 10.1175/JCLI-D-16-0115.1

Jeong et al. 2006). Some studies suggest that natural variability is the primary cause of cold events in East Asia. For example, Takaya and Nakamura (2005a,b) identified two typical types of anomalous circulation patterns that enhance the Siberian high and cause cold-air outbreaks in East Asia. The first is the ''wave train (Atlantic origin)'' type, which arises from the propagation of a quasi-stationary Rossby wave packet over Eurasia, along with the corresponding anticyclonic center that progresses slowly eastward. The second so-called ''Pacific origin'' type describes a slow retrogression of the main anticyclonic center from the northern North Pacific. A study by Park et al. (2008) investigated the atmospheric circulation associated with two cold surges during the 2005/06 winter, finding that the first cold surge was induced by the Pacific-origin type, and the second by the wave train type. Song et al. (2016) analyzed the intraseasonal variation of the strength of the East Asian trough. They found that prior to the peaks of strong East Asian trough events, an upper-level Rossby wave train propagated across northern Eurasia into East Asia and the northwestern Pacific.

Further studies suggest that cold events in East Asia may also be intensified by large-scale circulation anomalies (Jeong and Ho 2005; Park et al. 2011) as well as by remote forcing, such as sea surface temperatures (SSTs) (Zhang and Wang 1997; Chen et al. 2004) and Arctic sea ice loss (Wu et al. 2013; Tang et al. 2013; Zhang et al. 2016). For example, Park et al. (2011) investigated the relationship between East Asian cold surges and the Arctic Oscillation (AO) index. They divided East Asian cold surges into those associated with wave trains and those caused by anticyclonic blocks. While the blocking type generally occurs during the negative phase of the AO, the wave train type occurs during both phases of the AO. Chen et al. (2004) found that the North Pacific ENSO short wave train influences cold surges, while Tang et al. (2013) linked Arctic sea ice loss with the occurrence of extreme cold events in the northern continents. It has also been suggested that autumn Arctic sea ice loss promotes the occurrence of extreme negative phases of the tripole wind pattern during winter over Eurasia, which leads to cold-air outbreaks in East Asia (Wu et al. 2013).

The main goal of this study is to improve understanding of the causes and evolution of extreme cold spells in East Asia. We take two approaches: the first is a case study, in which we investigate dominant features of the intraseasonal evolution of winter atmospheric circulation anomalies associated with a cold event over the Asian continent from 17 January to 1 February 2012. This event lasted more than two weeks, distinguishing it from a short-lived synoptic cold surge process (Chang and Lau 1980, 1982). Second, we explore possible causes of similar cold events using model simulations forced by observed Arctic sea ice concentrations combined with different atmospheric initial conditions. Our results indicate that 1) the impact of atmospheric circulation anomalies over the northeastern Pacific–Aleutian region on Asian cold events (i.e., the downstream effect) plays a critical role; and 2) the combined impacts of both Arctic sea ice loss from August 2011 to February 2012 and the Arctic atmospheric circulation condition in the summer of 2011 were the main causes of this particular cold event.

2. Data and methods

The following datasets were used in this study: 1) monthly Arctic sea ice concentrations (SICs) and SSTs from 1979 to 2013 on a $1° \times 1°$ grid, obtained from the British Atmospheric Data Centre (BADC; Hadley Centre for Climate Prediction and Research 2006); 2) the daily sea level pressure (SLP), surface air temperatures (SATs), 10-m surface winds, and 1000- and 500-hPa geopotential heights from 1 January 1979 to 31 December 2012, obtained from the NCEP–NCAR reanalysis (http://iridl.ldeo.columbia.edu/SOURCES/NOAA/NCEP-NCAR/CDAS-1/DAILY/).

In this study, three indices are calculated by using winter (1 December–28 February of the next year; e.g., the winter of 2011/12 refers to December 2011–February 2012) daily SLP and SAT data: the Siberian high index (SHI), the SAT index (SATI), and the Aleutian low index (ALI). The SHI (SATI) is defined as the regionally averaged daily SLP (SAT) in the region bounded by 40°–60°N, 80°–120°E. The ALI is the regionally averaged daily SLP in the region 50°–70°N, 180°–150°W.

To explore a possible reason for the Asian cold event in January–February 2012, simulation experiments forced by observed Arctic SICs were conducted using the ECHAM5 (Roeckner et al. 2003) model (T63 spectral resolution and 19 pressure levels).

3. Atmospheric circulation anomalies associated with the 2012 cold event

In the winter of 2011/12, the seasonal-mean SHI was 1033.5 hPa, the highest value of 33 winters from 1979 to 2012. Persistent low temperatures over the Asian continent occurred from 17 January to 1 February, with a consecutive daily SATI below minus one standard deviation (-1σ; Fig. 1a). During 11–16 January the ALI rapidly weakened from 1005 to 1040 hPa, then quickly returned to 1005 hPa during 17–21 January, corresponding to the rapid strengthening of the Siberian high

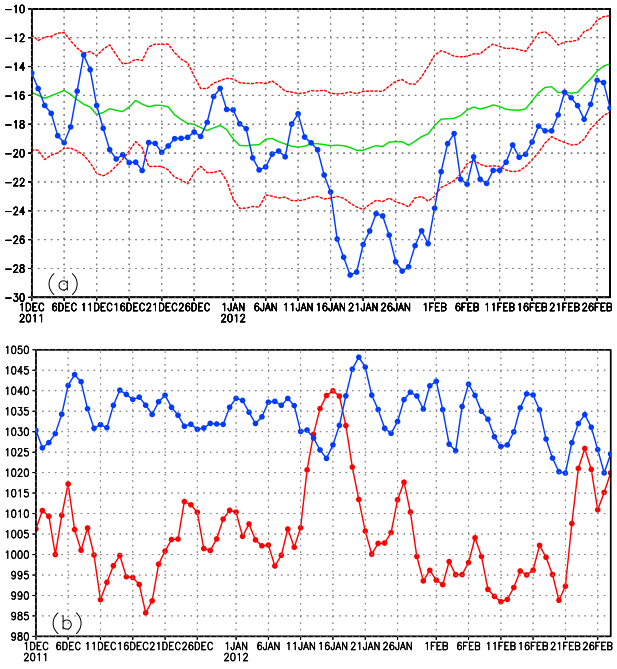

FIG. 1. (a) SAT averaged over the region bounded by 40°–60°N, 80°–120°E (SATI; °C). Blue line is for daily SATI values from 1 Dec 2011 to 28 Feb 2012, and the green line is for climatological values for these dates averaged over 1979–2012. Dashed red lines represent the daily climatological means plus or minus one standard deviation. (b) Daily SHI (blue) and ALI (red) for the same dates as in (a) (hPa). [The region bounded by the red (green) box in Fig. 2a is used to calculate SHI and SATI (ALI).]

(Fig. 1b). The subsequent reduction in the ALI was concurrent with outbreaks of the cold event. Ding and Krishnamurti (1987) and Ding (1990) indicated that strong diabatic cooling and a large-scale descent contributed to a rapid buildup of the Siberian high, which is often followed by cold surges over East Asia. Here we find, however, that when this cold event began (17 January), the intensity of the Siberian high was not particularly strong (Fig. 1b).

From 17 January to 1 February, negative SAT anomalies occupied most of Eurasia, with the anomaly center located in Siberia (<−8.0°C; Fig. 2a). Meanwhile, positive SAT anomalies appeared over the Nordic–Barents–Siberian marginal seas and far eastern Russia, with maximum values in the Barents–Kara Seas (>10°C). SAT anomalies are dynamically consistent with SLP and 500-hPa geopotential height anomalies (Figs. 2b,c). Positive SLP anomalies covered most parts of the mid- and high latitudes of Eurasia, with two anomaly centers near the Ural Mountains (>25 hPa) and in far eastern Russia (>10 hPa). At 500 hPa, geopotential height anomalies showed a tripole structure over Eurasia, with two negative anomaly centers located over eastern Europe and south of Lake Baikal, along with a dominant positive center over the Barents–Kara Seas and the Ural Mountains. After 1 February the extreme cold region slowly migrated westward and affected Europe (Fig. 2d).

An analysis of atmospheric circulation evolution before the cold event (Fig. 3) helps us understand its formation process and potential precursors. During 5–7 January, positive SLP anomalies existed over much of the Asian continent, northwestern Pacific, northeastern North Atlantic (>20 hPa), and northeastern Pacific (>10 hPa). Negative anomalies were evident in Europe, parts of the Arctic, and over much of North America (Fig. 3a). During 8–10 and 11–13 January, positive SLP anomalies had weakened over Asia, while positive SLP anomalies strengthened and shifted northward in the northeastern Pacific (Figs. 3b,c). During 14–16 January, positive SLP anomalies occupied most of the northern North Pacific, peaking at greater than 40 hPa (Fig. 3d). Meanwhile, in the northeastern North Atlantic, positive SLP anomalies shifted northeastward and connected with anomalies in the Aleutian region. Positive anomalies also strengthened over northern Asia, particularly east of the Ural Mountains, with negative anomalies elsewhere in Asia.

In the early stage of the cold event (17–19 January), the center of positive SLP anomaly over the Aleutian region weakened and shifted northwestward toward the Bering Strait (Fig. 3e). Simultaneously, positive SLP anomalies formed over nearly the entire Asian continent north of 40°N, generating a center east of the Ural Mountains (>20 hPa), indicating a rapid strengthening of the Siberian high. In East Asia, positive SLP anomalies from the Aleutian region extended southwestward to near 30°N. During 20–22 January, the anomalous center from the Bering Strait (17–19 January) migrated southwestward to the Kamchatka Peninsula and its strength weakened further (Fig. 3f). The southwestward propagation of SLP anomalies is consistent with previous studies (Branstator 1987; Kushnir 1987; Takaya and Nakamura 2005b).

During 23–25 January, the core of positive SLP anomalies retreated northward of 50°N over the Asian continent, and its center over the Ural Mountains intensified and also migrated farther northward (Fig. 3g). From 23–25 to 29–31 January, positive SLP anomalies strengthened rapidly and extended westward over northern Eurasia and the Arctic. Meanwhile, positive SLP anomalies over the Bering Sea and far eastern Russia gradually retreated westward (Figs. 3g–i). Positive SLP anomalies clearly propagated westward over the Pacific sector and Eurasia (Fig. 3), consistent with the SAT evolution shown in Figs. 2a,d.

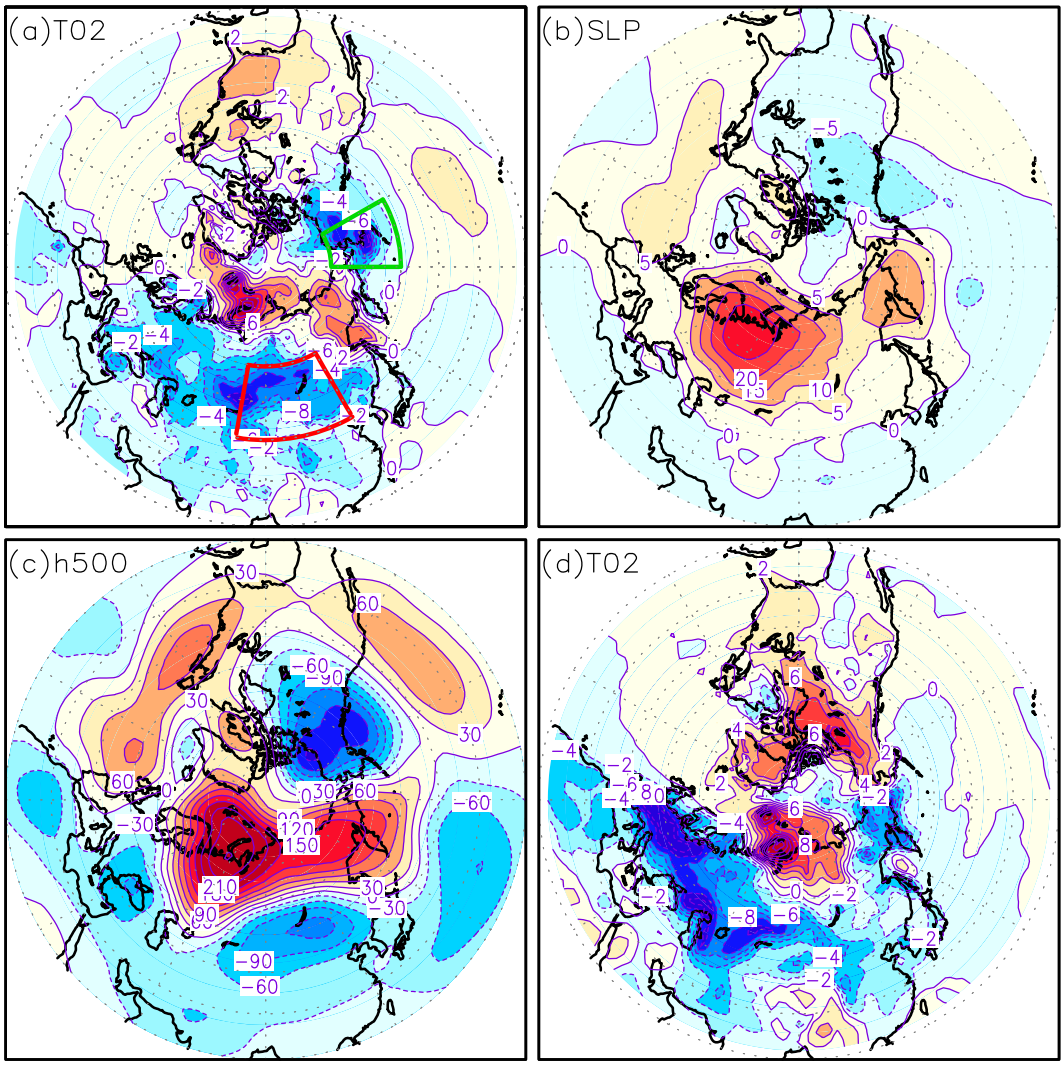

FIG. 2. (a) SAT anomalies (relative to the 1979–2012 mean) averaged from 17 Jan to 1 Feb 2012. (b),(c) As in (a), but for SLP and 500-hPa geopotential height anomalies. (d) As in (a), but from 2 to 11 Feb 2012. Contour intervals are 2°C in (a) and (d), 5 hPa in (b), and 30 gpm in (c). The red and green boxes in (a) are boundaries of 40°–60°N, 80°–120°E (SHI and SATI) and 50°–70°N, 150°W–180° (ALI), respectively.

The evolution of 500-hPa geopotential heights displayed distinct features (Fig. 4). During 5–7, 8–10, 11–13, and 14–16 January, geopotential heights exhibited a multipole structure over the high latitudes, with ridges over the northeastern North Atlantic, central Eurasia, and northeastern Pacific (Figs. 4a–d). A particularly sharp ridge formed along the North American west coast during 14–16 January, which then cut off from the main flow and became a persistent blocking high over far northeastern Siberia. During 17–19 January, two ridges over Eurasia and the Pacific further developed and generated two closed centers; the latter became a polar blocking high with central geopotential heights exceeding 5600 gpm. A similar spatial pattern was observed in 20–22 January (Figs. 4e,f). The evolution of atmospheric circulation over Alaska and eastern Siberia (Figs. 4d and 4e, respectively) resembles the Pacific-origin type (Takaya and Nakamura 2005b). The wavy signature over Eurasia (Figs. 4e,f), however, is typical of the Atlantic-origin type (Takaya and Nakamura 2005a). Along the eastern margin of the Eurasian blocking high, northerly winds advected cold air from high latitudes into central Asia, leading to the strengthened Siberian high (Figs. 3e,f) and negative SAT anomalies there. Meanwhile, the polar blocking high over far eastern Russia prevented cold air masses from departing East Asia (Fig. 4f).

During 23–25 January, the geopotential height pattern (Fig. 4g) resembled that during 20–22 January, but

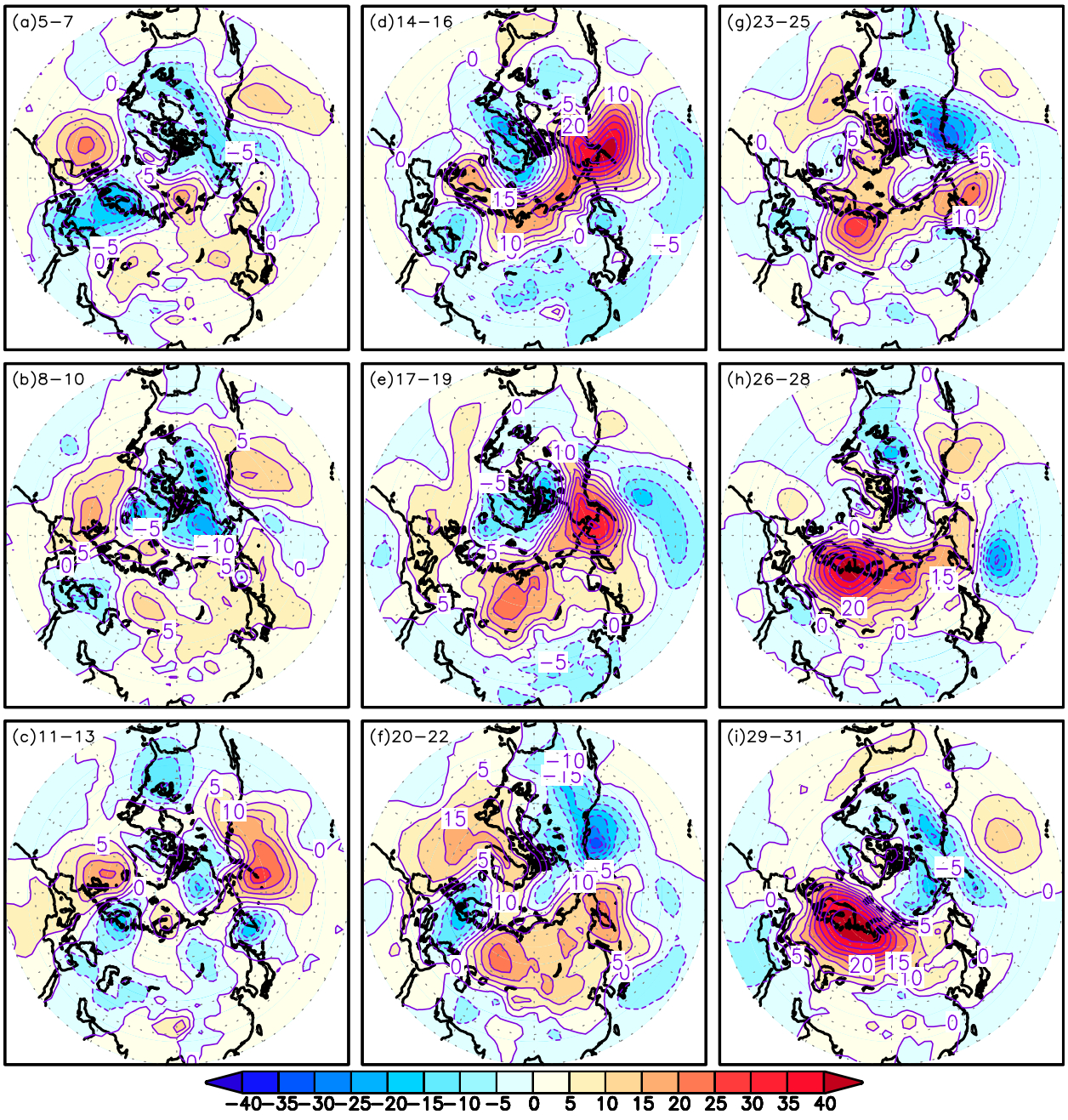

FIG. 3. Evolution of SLP anomalies (relative to the 1979–2012 mean) during January 2012. (a) SLP anomalies averaged over 5–7 Jan. (b)–(i) As in (a), but for 8–10, 11–13, 14–16, 17–19, 20–22, 23–25, 26–28, and 29–31 Jan, respectively. Date ranges in January are indicated on each plot. Contour intervals are 5 hPa.

with a weakened and northward-migrated Eurasian blocking high and a weakened and southward-shifted polar blocking high. Through 26–31 January, the Atlantic ridge rapidly developed and connected with the Eurasian blocking high (Figs. 4h,i). This cold event peaked twice in January: during 17–22 and again during 25–29 January (Fig. 1a). Although the corresponding circulation patterns in both SLP and 500-hPa geopotential heights were, to some extent, similar over the Asian continent, their differences also were dominant over the northern North Pacific and the Arctic.

Prior to the cold outbreak, the upper-level wave activity flux (WAF) (Takaya and Nakamura 2001) propagated from the northeastern North Atlantic across Europe into the low latitudes of the Asian continent (Figs. 5a–d). At the time of the outbreak, the WAF into the low latitudes of the

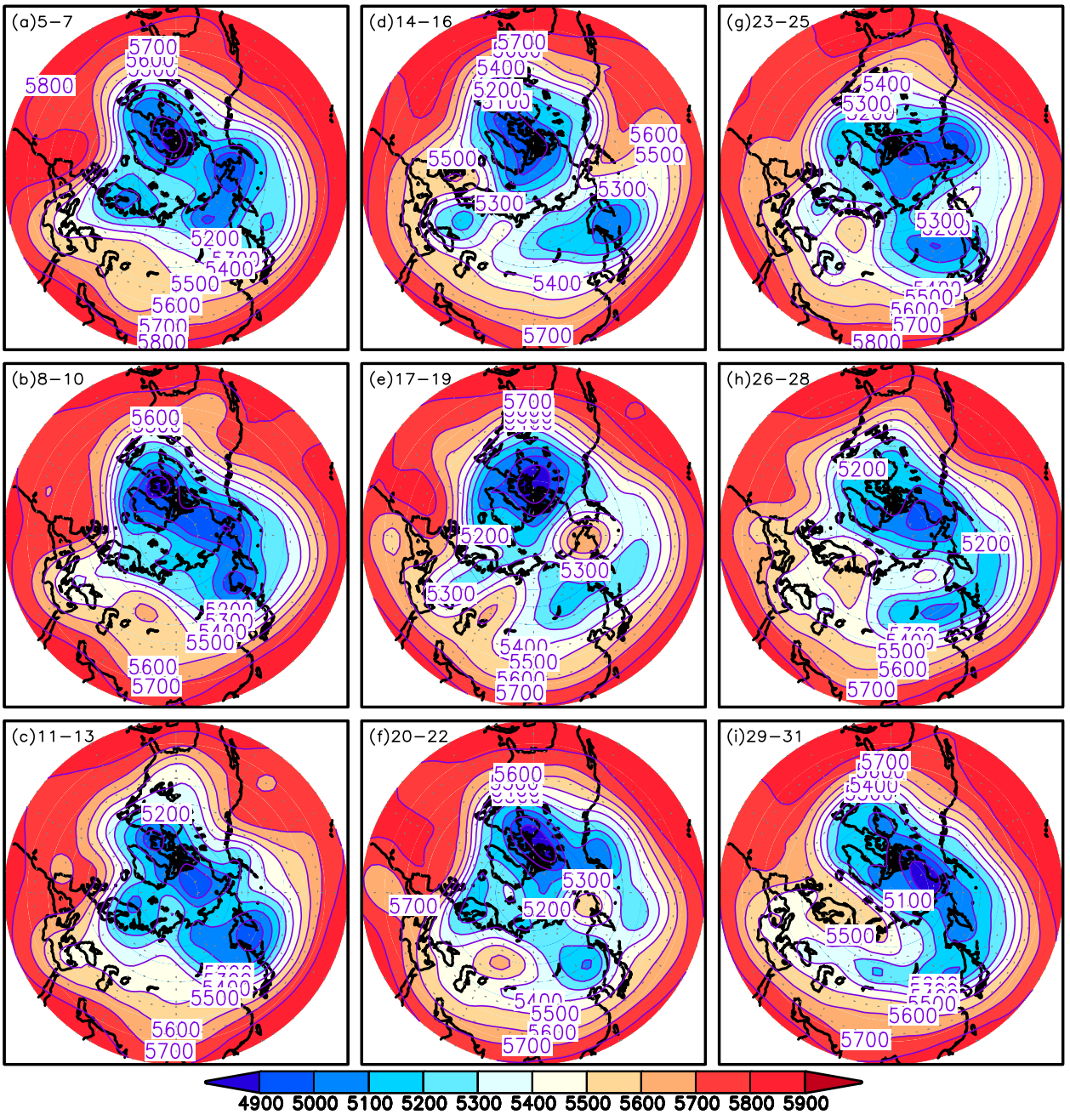

FIG. 4. As in Fig. 3, but for 500-hPa geopotential height fields, contour intervals are 100 gpm.

Asian continent weakened rapidly while the propagation over the mid- and high latitudes of the Asian continent became dominant. Additionally, over the North Pacific, the WAF gradually concentrated in the northern North Pacific Fig. 5e). After the outbreak, the WAF propagation remained over the northern North Pacific and vicinity (Figs. 5f,g). After 26 January, the WAF weakened over the Asian continent (Figs. 5h,i). These analyses suggest that the evolution of atmospheric features over the northeastern North Atlantic and northeastern Pacific may provide important precursors for this cold event, particularly the formation of the blocking highs that were key to the flow of Arctic air masses into central Asia as well as for creating a persistent pattern.

To better understand possible causes for this cold event, it is necessary to analyze seasonal and monthly atmospheric circulation anomalies during the winter of 2011/12, which can be used to assess the realism of

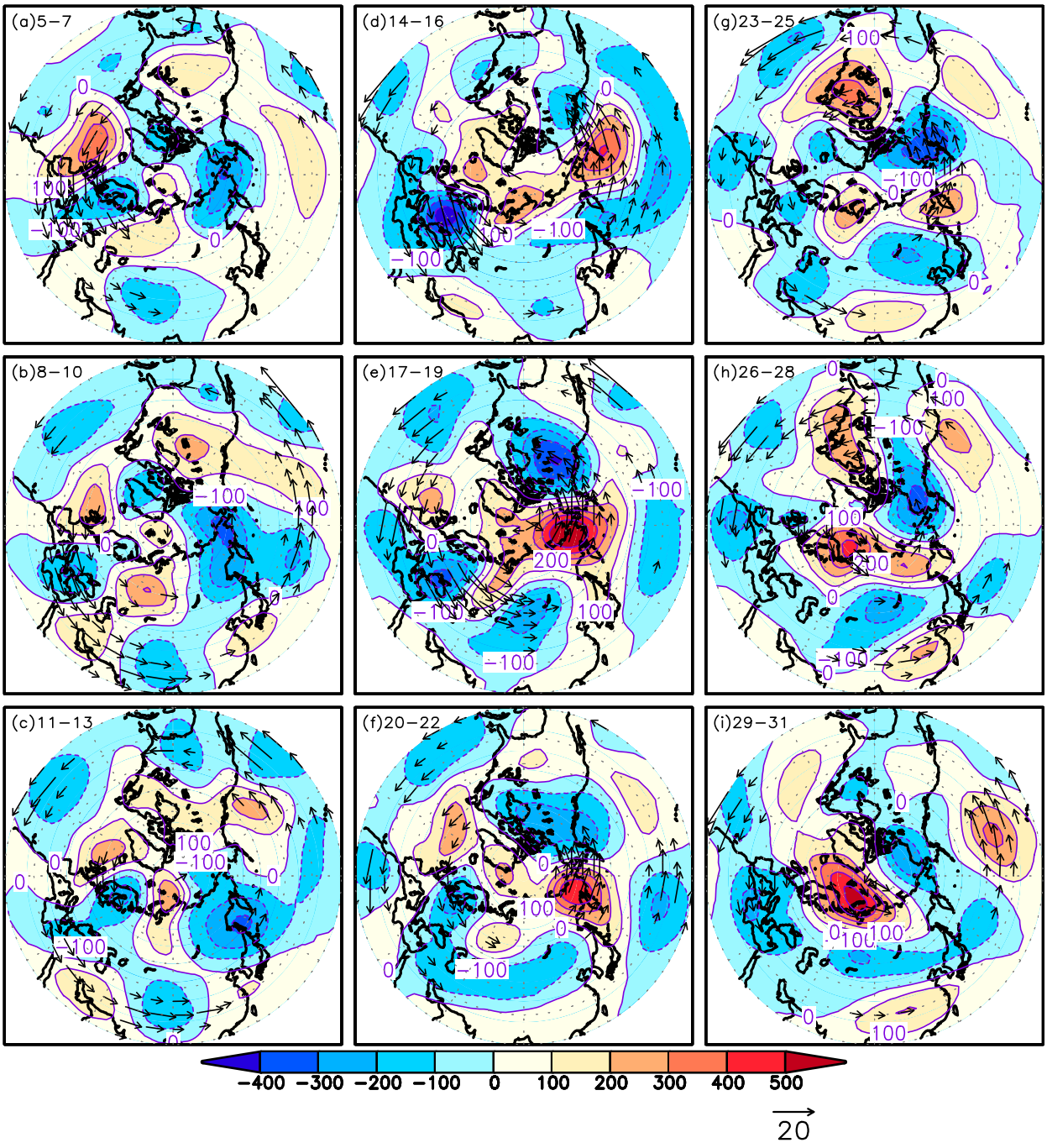

FIG. 5. As in Fig. 3, but for 200-hPa geopotential height anomalies (contours), superimposed on the wave activity flux (arrows, $m^2 s^{-2}$) of Takaya and Nakamura (2001). Shaded intervals are 100 gpm.

simulation experiments and their ability to reproduce the major atmospheric features observed in this extreme winter. Dominant features were a strengthened Siberian high and a positive AO phase, with three positive SLP centers over the Ural Mountains, northeastern North Atlantic, and northeastern Pacific (Fig. 6a). We note that a similar but weaker SLP pattern occurred in December 2011, but positive SLP anomalies were relatively weak over the Ural Mountains (Fig. 6b). In January 2012, SLP anomalies exhibited a dumbbell structure over northern Eurasia and the Aleutian region (Fig. 6c), closely resembling the pattern shown in Fig. 2b. This implies that these features can be attributed mainly to anomalies associated with the cold event,

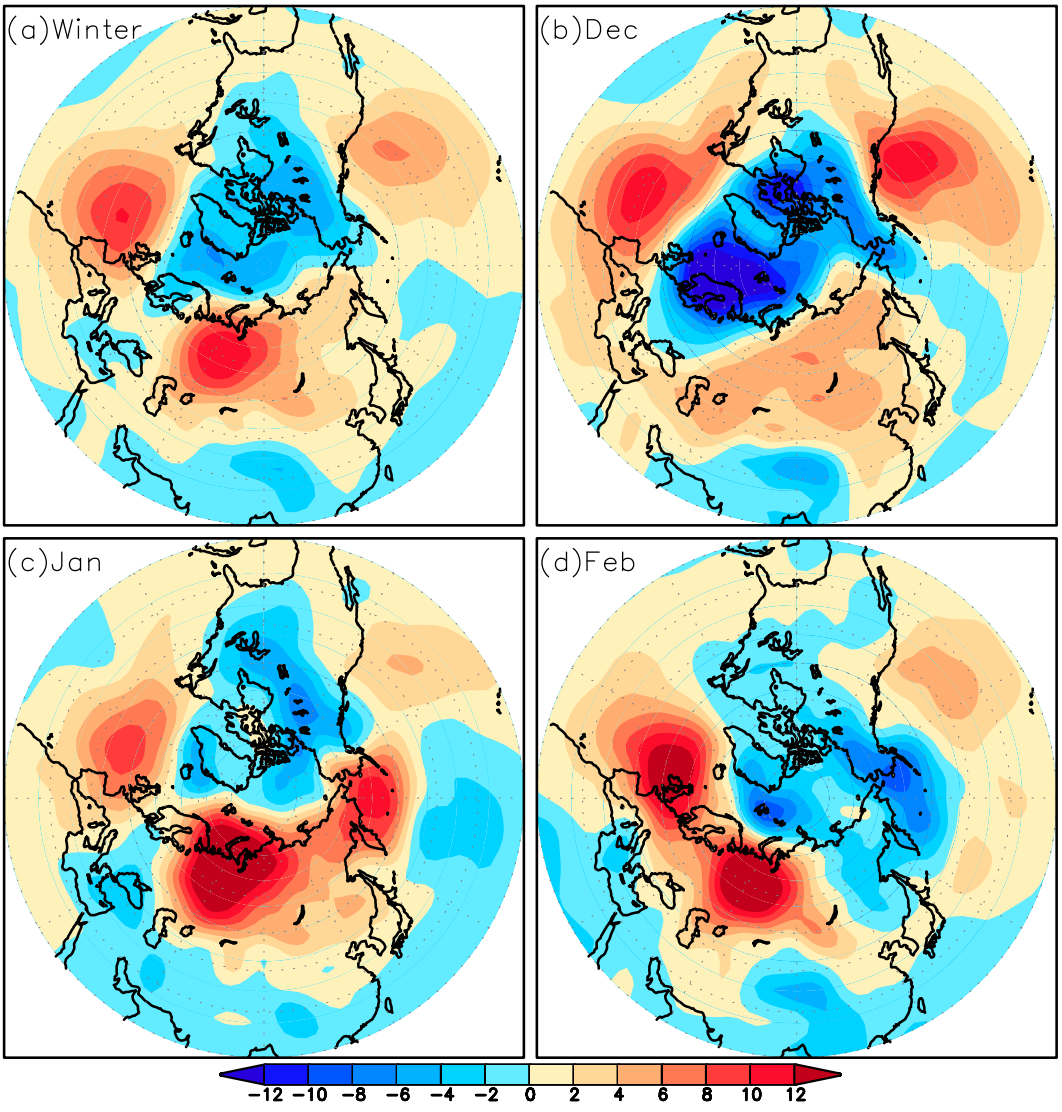

FIG. 6. (a) Observed SLP anomalies in the winter of 2011/12, relative to the 1979–2012 mean. (b) As in (a), but for December 2011, relative to the 1979–2011 mean. (c) As in (a), but for January 2012, relative to the 1980–2012 mean. (d) As in (c), but for February 2012. Contour intervals are 2 hPa.

consistent with previous studies (Meehl et al. 2001; Davies 2015). In February 2012, positive SLP anomalies appeared mainly over the Ural Mountains and the northeastern North Atlantic, along with a deep Aleutian low (Fig. 6d). In the mid- and high latitudes of Eurasia, seasonal and monthly SLP patterns arise in part owing to impacts of persistent weather patterns (Figs. 3 and 6), particularly in January 2012 (Figs. 2b, 3, and 6c).

4. Did Arctic sea ice loss play a role?

Many studies have demonstrated that Arctic sea ice loss contributes to cold Eurasian winters through effects on jet-stream dynamics and/or a possible stratosphere–troposphere interaction (Alexander et al. 2004; Deser et al. 2004; Magnusdottir et al. 2004; Honda et al. 2009; Petoukhov and Semenov 2010; Wu et al. 2011, 2013; Francis and Vavrus 2012, 2015; Liu et al. 2012; Jaiser et al. 2013; Tang et al. 2013; Cohen et al. 2014; Mori et al. 2014; Nakamura et al. 2015; Kug et al. 2015; Li et al. 2015). Other studies, however, reported uncertainty in these associations (Screen and Simmonds 2013a,b; Screen et al. 2014; Perlwitz et al. 2015; Overland et al. 2015; Walsh 2014; Wu et al. 2015; McCusker et al. 2016; Meleshko et al. 2016). Here we investigate, through observations and model experiments, whether patterns

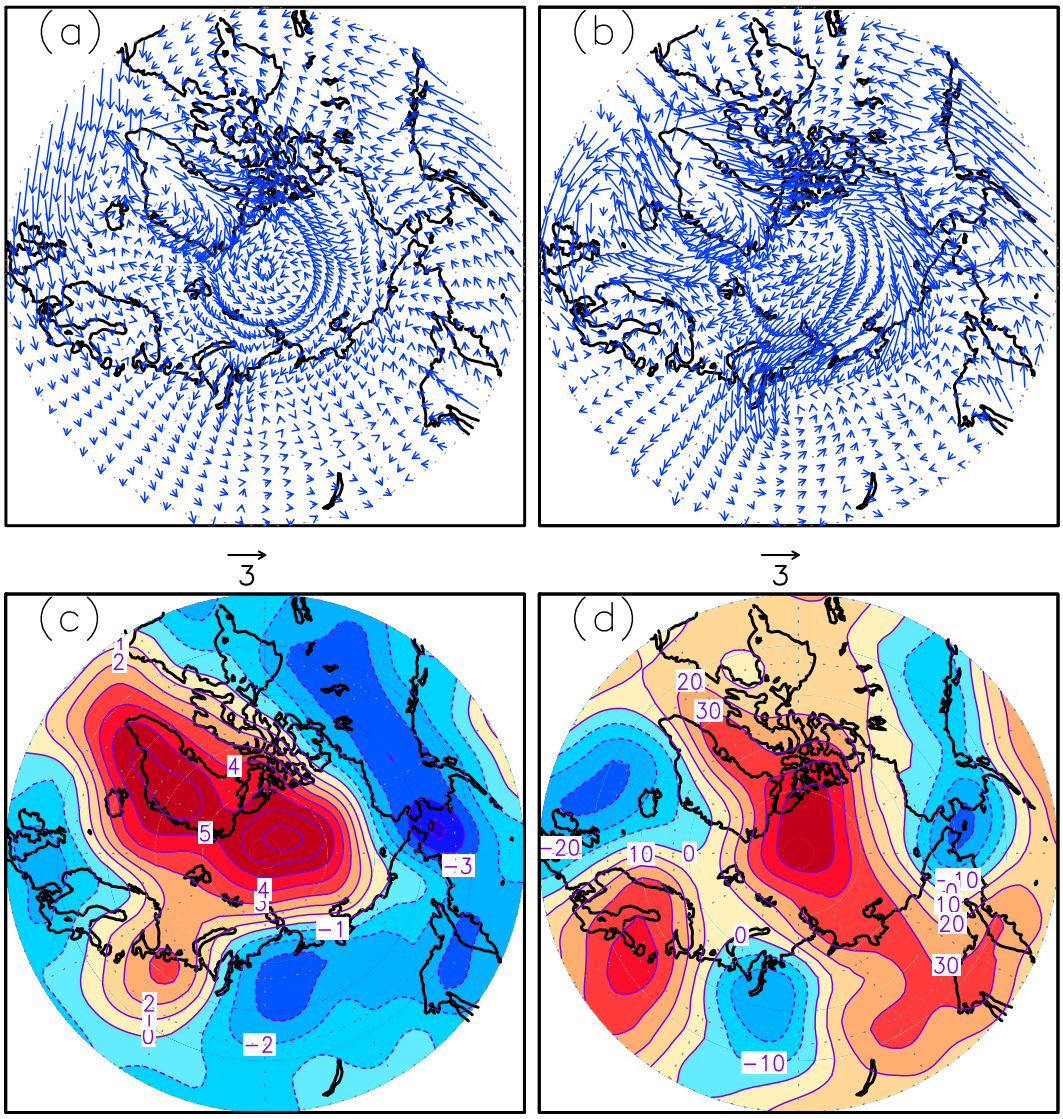

FIG. 7. (a) Climatological summer (JJA) 10-m winds (m s^{-1}) averaged over 1979–2012. (b) Mean summer 10-m winds in 2011. (c) Summer SLP anomalies (hPa) in 2011 (relative to the 1979–2012 mean). (d) As in (c), but for 1000–500-hPa thickness anomalies (gpm).

of sea ice loss from summer to the following winter may have contributed to the atmospheric evolution that led to the 2012 cold event. Consequently, it is necessary to understand the main features of the summer atmospheric circulation in 2011 over the Arctic.

Observed mean surface winds during summers from 1979 to 2012 (Fig. 7a) exhibited a weak cyclonic flow over most of the Arctic Ocean, a pattern that does not favor sea ice loss (Ogi et al. 2010; Overland et al. 2012; Wu et al. 2012). In contrast, surface winds in the summer of 2011 (Fig. 7b) showed a strong anticyclonic pattern, which is typically associated with sea ice loss in summer, thus contributing to a reduced ice cover in the summer of 2011 (Ogi et al. 2010; Wu et al. 2012). Positive SLP anomalies covered most of the Arctic Ocean, Greenland, and North Atlantic, along with negative anomalies elsewhere (Fig. 7c). Positive thickness anomalies also prevailed, indicating warm conditions in high latitudes (Fig. 7d).

Spatial distributions of Arctic SIC anomalies from the summer of 2011 to the ensuing winter are presented in Fig. 8. Decreased summer SICs are apparent in the marginal seas from the Barents Sea counterclockwise to the Beaufort Sea, which corresponds with the anticyclonic wind pattern (Figs. 8a and 7b). Summer surface winds enhanced sea ice fracturing and ocean mixing, which promoted further melting and expansion of open water (Ogi et al. 2010; Spreen et al. 2011; Wu et al. 2012). During autumn the spatial distribution of decreased

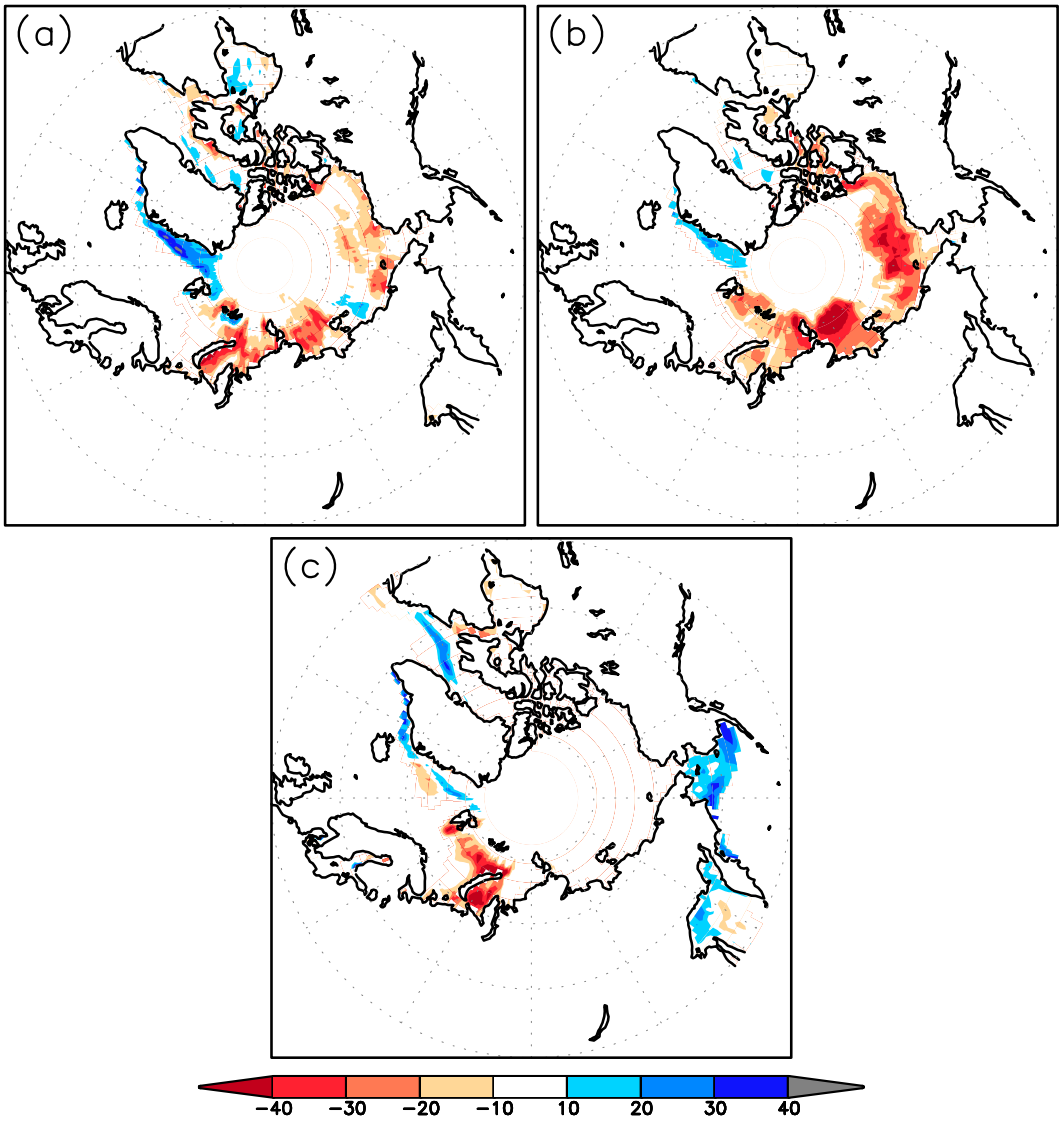

FIG. 8. (a) SIC anomalies (%) in the summer (JJA) of 2011 (relative to the 1979–2012 mean). (b),(c) As in (a), but for SIC anomalies in the autumn (SON) of 2011 and in the winter (DJF) of 2011/12 (relative to the 1979–2013 mean), respectively.

SICs was similar to the previous summer, but with expanded and stronger negative anomalies (Fig. 8b). In the following winter, decreased SICs were confined to the Barents–Kara Seas, while increased SICs mainly occurred in the Bering Sea (Fig. 8c).

To investigate combined impacts of Arctic sea ice loss and Arctic atmospheric circulation in the summer of 2011 on cold events in wintertime, two sets of simulation experiments were conducted. The motivation for these experiments is to demonstrate that these two factors could lead to the favorable wintertime circulation that facilitate the occurrence of cold events resembling the cold event in 2012. The first experiment (E1) was performed with observed monthly SICs in the Northern Hemisphere from August 2011 to March 2012 as the external forcing, while the SICs in the Southern Hemisphere and global SSTs were prescribed as their climatological monthly means. The SSTs and SICs were spatially interpolated from observations obtained from the BADC [details are available from the Atmospheric Model Intercomparison Project (AMIP) II SSTs and SICs boundary condition dataset (http://www-pcmdi.llnl.gov/projects/amip/AMIP2EXPDSN/BCS/bcsintro.php)]. In regions where the SIC varies year to year, SSTs were prescribed at climatological values. This experiment was repeated with 92 different atmospheric initial conditions

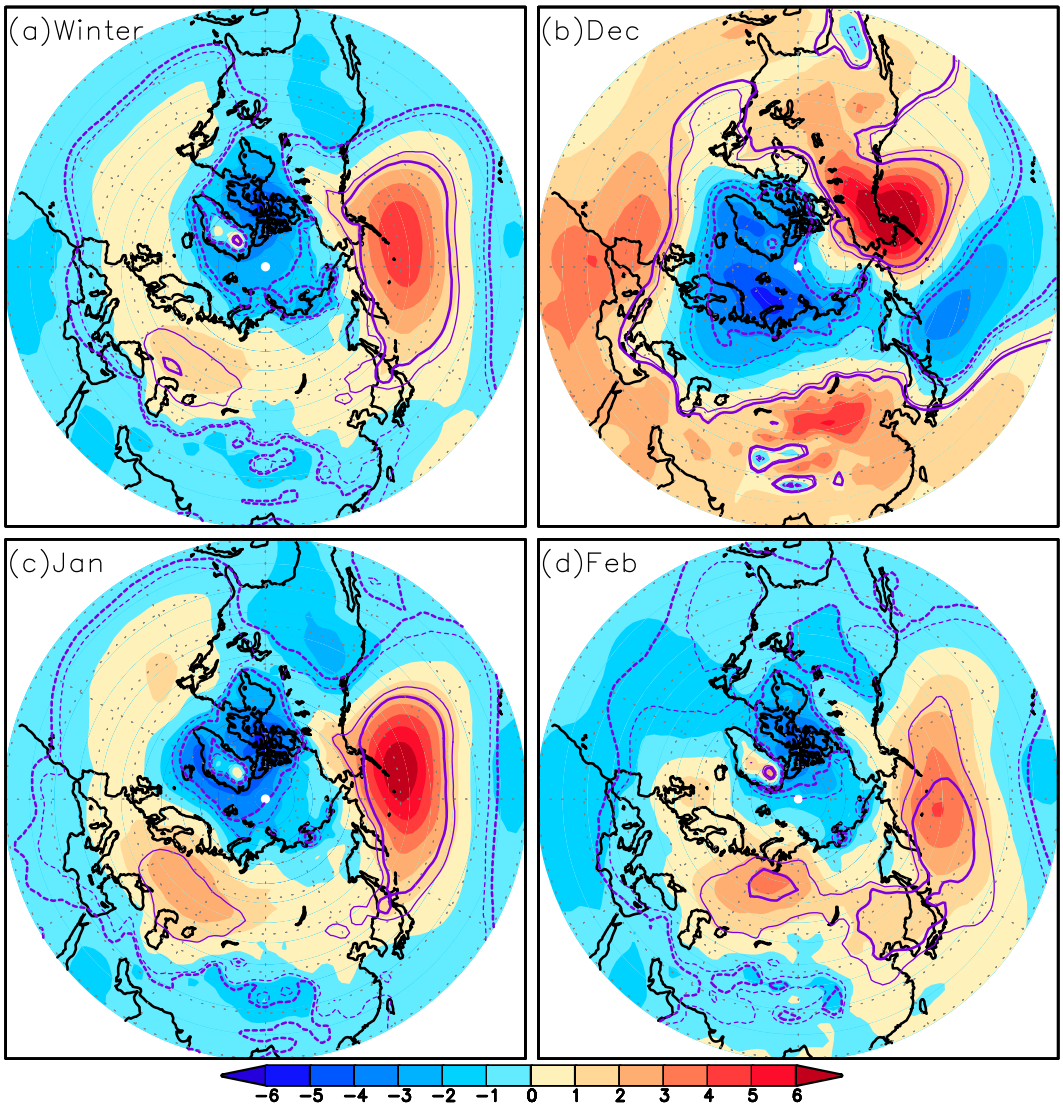

FIG. 9. (a) Simulated winter mean SLP differences derived from ensemble means of 92 winters in E1 minus the control run. Thin and thick purple (dashed and solid) contours denote SLP differences at the 0.05 and 0.01 confidence levels, respectively. (b)–(d) As in (a), but for December 2011, January 2012, and February 2012, respectively. Shaded intervals are 1 hPa.

during summer (JJA) 2011 obtained from spatially interpolated daily NCEP–NCAR reanalysis values. Variables include surface pressure, air temperature, divergence, vorticity, and specific humidity.

The second experiment (E2) was carried out by prescribing observed monthly SICs in the Northern Hemisphere from January 1978 to December 2013 as the external forcing. The SICs in the Southern Hemisphere and global SSTs were the same as in E1. This experiment was repeated with 10 different atmospheric initial conditions that were derived from a control run, which contained 60 years of simulations with SICs and SSTs prescribed as their climatological monthly means. Thus, the model output in E2 contained 350 winters (31 500 days). Differences between these two experiments will illuminate roles of different initial atmospheric conditions in influencing the atmosphere's response to sea ice conditions during winter 2011/12.

Can the model capture the major seasonal and monthly atmospheric features observed in the winter of 2011/12? This question is critical for determining whether Arctic sea ice loss contributed to the cold event. Our analysis focuses on SLP responses during wintertime because the southward outbreak of polar air masses is closely associated with winter SLP anomalies. Simulated (E1) SLP anomalies during winter (Fig. 9a) feature

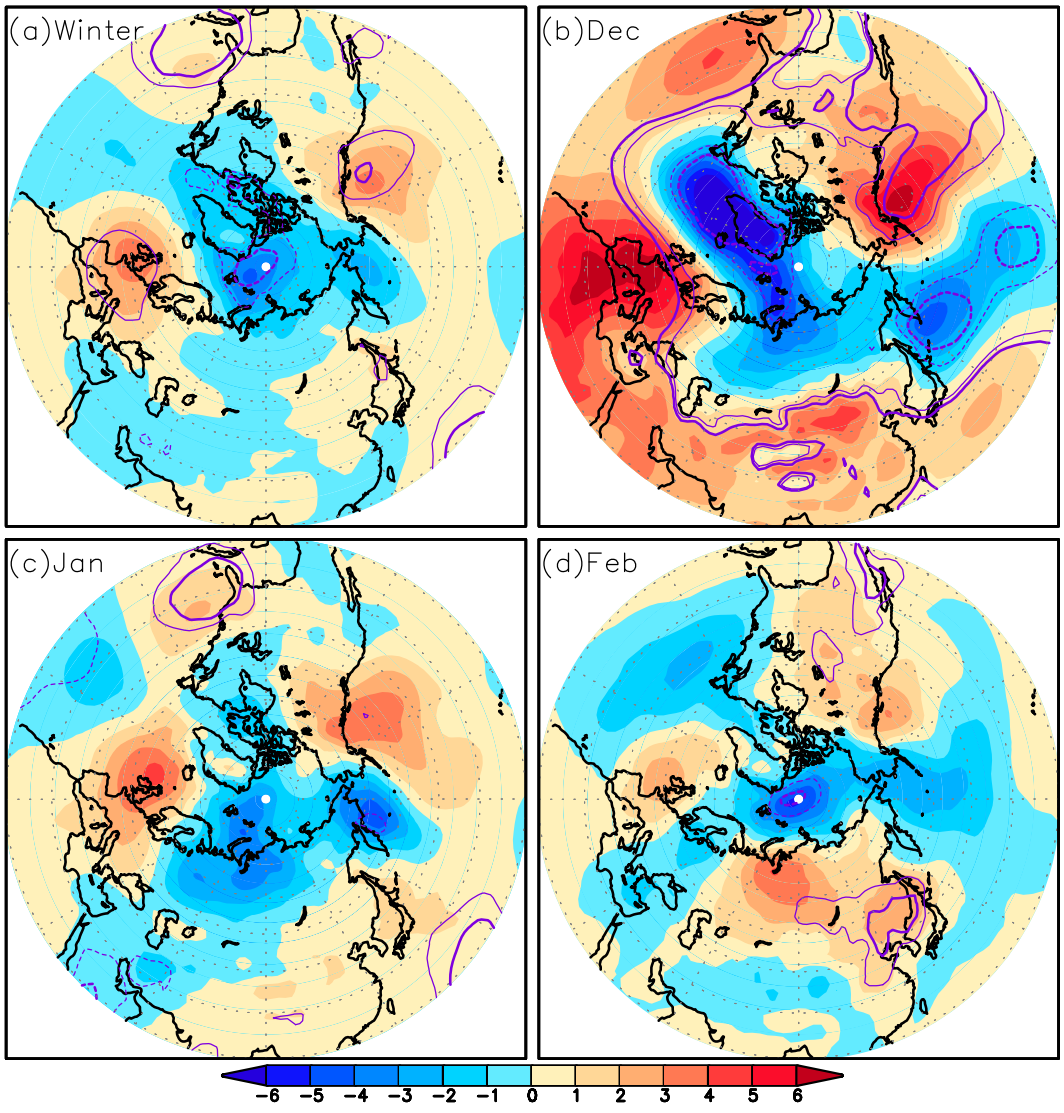

FIG. 10. As in Fig. 9, but for E2 minus the control run.

positive values in a belt from the east coast of North America across the northern North Atlantic and Eurasia to the northern North Pacific, with centers over the Aleutian region (>4 hPa) and central Eurasia north of the Caspian Sea (>1 hPa). Meanwhile, negative SLP anomalies prevail over the Arctic, North America, and south of the positive belt. This pattern is somewhat reminiscent of the positive phase of the AO, and is consistent with observed SLP anomalies during winter 2011/12 (Fig. 6a). Simulated positive SLP anomalies over central Eurasia and the northern North Atlantic are weaker than in observations, while anomalies over the North Pacific are stronger. During the month of December 2011, simulated SLP anomalies closely resemble observations (Figs. 9b vs 6b). SLP responses in January 2012 closely resemble winter-mean responses spatially, but feature large amplitudes (Fig. 9c), consistent with observations (Figs. 6a,c). In February 2012, simulated positive SLP anomalies exhibit a ''V'' structure extending across northern Eurasia, along the East Asian coast, and across the North Pacific, somewhat similar to observations (Figs. 9d vs 6d). The E1 simulations, therefore, capture most major features in the observed winter SLP patterns, implying that Arctic SIC anomalies from August 2011 to February 2012, together with specific atmospheric initial conditions in the preceding summer, contributed to the SLP anomalies observed during the winter of 2011/12. In particular, the E1 clearly indicates that a persistently weakened

Aleutian low is a dominant feature in winter SLP responses to sea ice loss, which is likely due to the accumulated impact of individual weather systems.

SLP anomalies from the E2 simulations for winter 2011/12 clearly differ from those in E1 because of the different summer atmospheric conditions (Figs. 10 vs 9). In contrast to E1, the E2 response does not exhibit a significantly weakened Aleutian low in any winter month. The different response suggests that ice conditions from August 2011 to February 2012 and initial conditions of the atmosphere led to a response that favors a strengthened Siberian high and weakened Aleutian low, which favor the occurrence of cold-air outbreaks over East Asia.

We now focus on simulations of the ALI. Output from the E1 includes 92 winters from 1 December to 28 February. The winter daily ALI was calculated and then ranked in order from the maximum to the minimum (i.e., from anomalously weak to strong Aleutian low). An ALI $\geq$ 1032.71 hPa corresponds to patterns with the probability of occurrence less than 10% (i.e., an extremely weakened Aleutian low). This analysis was repeated for the E2, with the result that the probability of occurrence less than 10% corresponds to the ALI $\geq$ 1031.51 hPa. Figure 11a shows probability distribution curves of the simulated winter daily ALI. We find that atmospheric initial conditions in the summer of 2011 strongly influenced the winter Aleutian low response to Arctic sea ice loss, leading to the probability distribution systematically shifting toward weak Aleutian lows. The probability of the ALI falling between 1033 to 1043 hPa was larger for the E1 than the E2, even in the winters of 2007/08 through 2012/13 when sea ice loss was robust (Fig. 11b). Moreover, under the same SIC forcing from August 2011 to March 2012, the simulated probability of the ALI $\geq$ 1032.71 hPa in the E1 (E2) was 9.97% (7.78%). Under the same Arctic sea ice conditions, therefore, atmospheric initial conditions in the summer of 2011 not only enhanced impacts of sea ice loss on winter atmospheric variability over Eurasia and North America (consistent with Wu et al. 2016), but they also strengthened a negative feedback on the Aleutian low [the negative feedback of sea ice loss generally refers to positive SLP (or geopotential height) anomalies produced by sea ice loss].

Finally, we focus on extreme cold events in the simulations. To qualify as an extreme cold event in the E1, it must satisfy the following three conditions: 1) the SATI ≤ -21.18°C (the probability of occurrence <10%) and the ALI $\geq$ 1032.71 hPa, 2) the event persists longer than 3 days, and 3) the interval between two extreme cold events exceeds 15 days. Following these criteria, 10 extreme cold events were

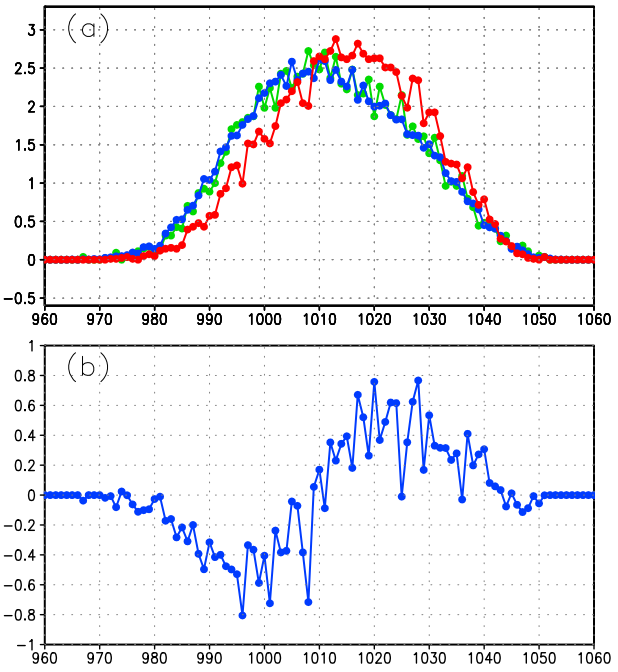

FIG. 11. (a) Probability distribution curves of simulated winter daily ALI (%) in E1 (red), E2 (blue), and six winters (2007/08–2012/13) from E2 (green). (b) Differences in probability distributions of simulated winter daily ALI between E1 [red curve in (a)] and 6 winters (2007/08–2012/13) of E2 [(green in (a)].

detected during the simulated winter of 2011/12, 9 of which occurred in January and 1 that occurred in February. This result was consistent with observations and simulations of strong Siberian high features in Figs. 6c and 9c that are associated with extreme cold events.

In Fig. 12 we present composite SLP anomaly fields for the 10 extreme cold events in E1 simulations corresponding to 3-day averages before and after the outbreak of the event. The center of the positive SLP anomaly over North America during 12–10 days before the event (Fig. 12a) shifted clockwise (westward) through time until it reached the Aleutian region in 3–1 days (Figs. 12b–d). Its strength gradually increased over this evolution, peaking in 0–2 days (Fig. 12e). Meanwhile, the positive SLP anomaly that began over eastern Europe progressed eastward toward Japan, intensified, and increased in size over the same time period. Since the 3–5 days after the breakout of the event, weakened and southwestward-extended SLP anomalies were observed over the Aleutian region and northwestern Pacific (Figs. 12f–i).

Although the evolution of ensemble-mean 500-hPa geopotential height anomalies in E1 simulations displayed some similarity to observations, they did not reproduce a polar blocking high or a multipole structure

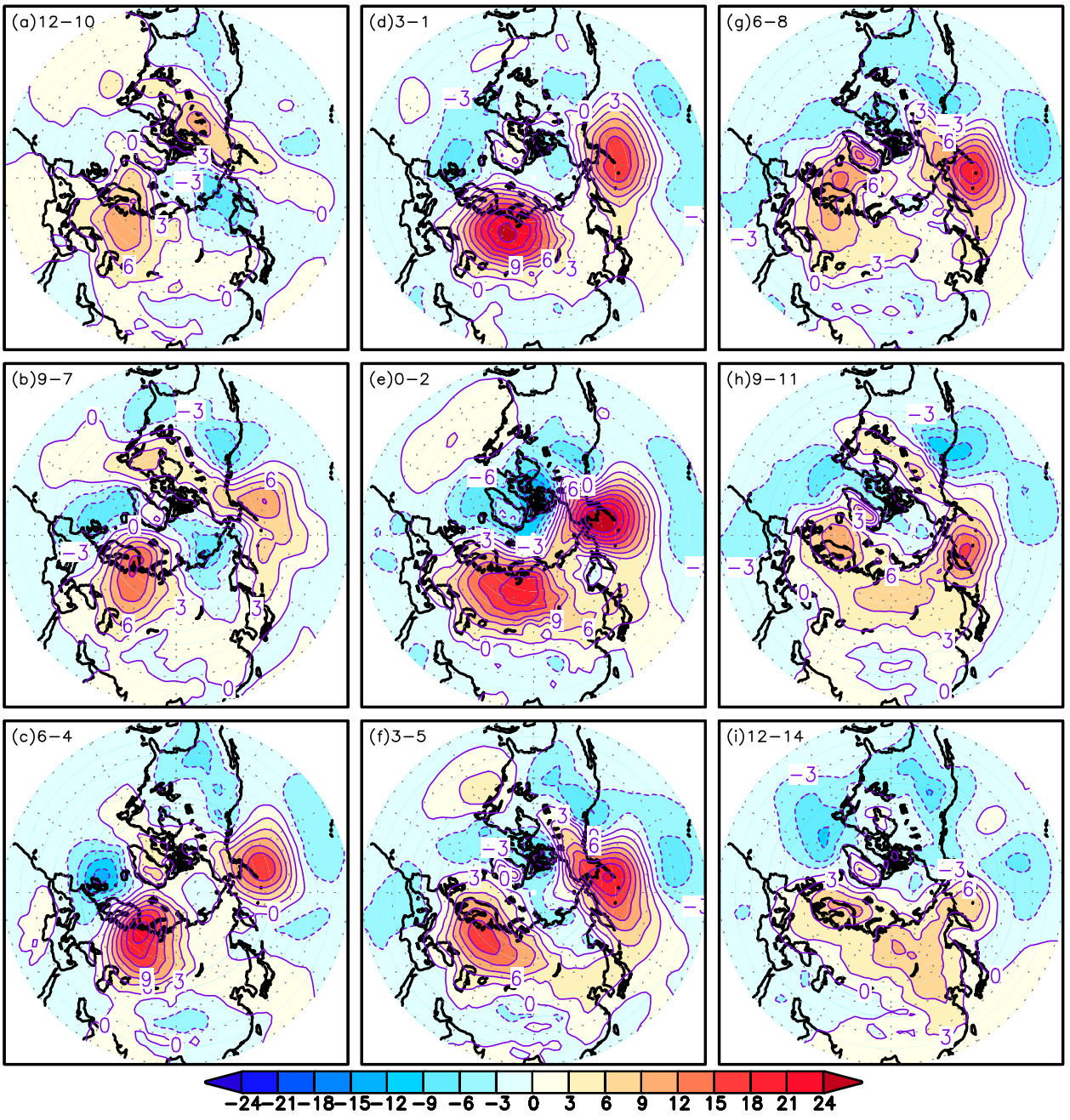

FIG. 12. Evolution of composited simulated winter daily SLP anomalies for selected 10 extreme cold events, derived from E1 minus the control run. (a) SLP anomalies averaged from 12 to 10 days prior to the extreme cold events. (b)–(d) As in (a), but for 9–7, 6–4, and 3–1 days prior to the extreme cold events, respectively. (e)–(i) As in (a), but for 0–2, 3–5, 6–8, 9–11, and 12–14 days after the peak of the extreme cold events, respectively. Contour intervals are 3 hPa.

in the high latitudes (not shown). Some individual members, however, did reproduce these features.

We now explore the behavior of the WAF during the 10 extreme cold events in E1 simulations. Figure 13 presents composited 200-hPa geopotential height anomaly fields superimposed on the WAF for the 10 extreme cold events. Over the northern North Pacific and East Asia, the positive center of geopotential height anomalies expanded westward, while undergoing a gradual strengthening (Figs. 13a–c), stable period (Figs. 13d–g), and then weakening (Figs. 13h,i), resembling the evolution of simulated SLP anomalies

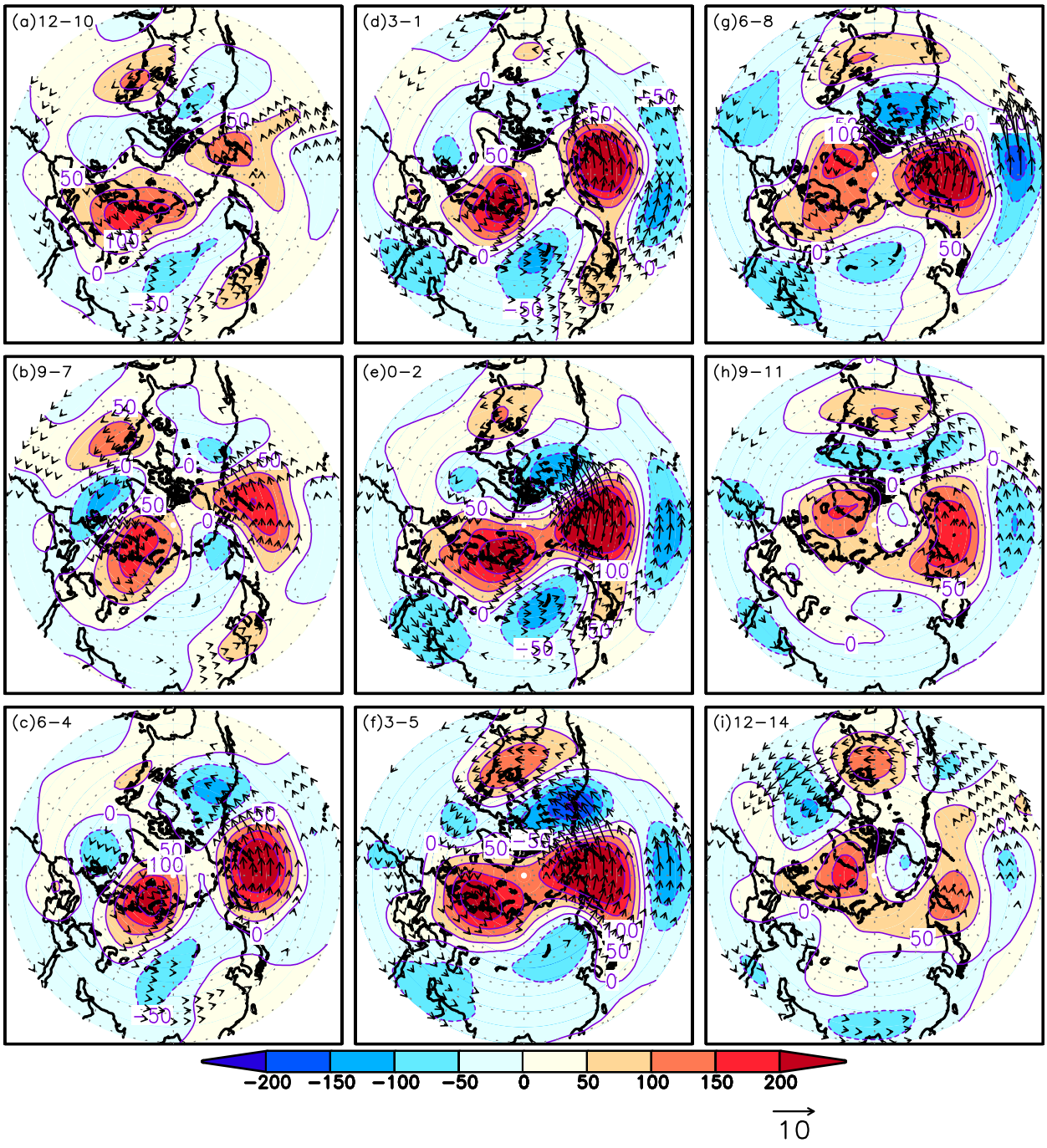

FIG. 13. As in Fig. 12, but for composited simulated winter daily 200-hPa geopotential height anomalies (contours), superimposed on the wave activity flux (arrows, $m^2 s^{-2}$) of Takaya and Nakamura (2001). Contour intervals are 50 gpm.

(Fig. 12). Meanwhile, a positive center over Eurasia and parts of the Arctic also exhibited intensification then stability, followed by a weakening and migration westward. Compared with the observations (Fig. 5), simulated 200-hPa geopotential height anomalies captured some of the major features, particularly over the northern North Pacific and East Asia. Simulated positive anomalies over Eurasia and parts of the Arctic, however, are clearly stronger than those in observations. The simulated WAF also bears some similarity to observations, particularly over the North Pacific and East Asia.

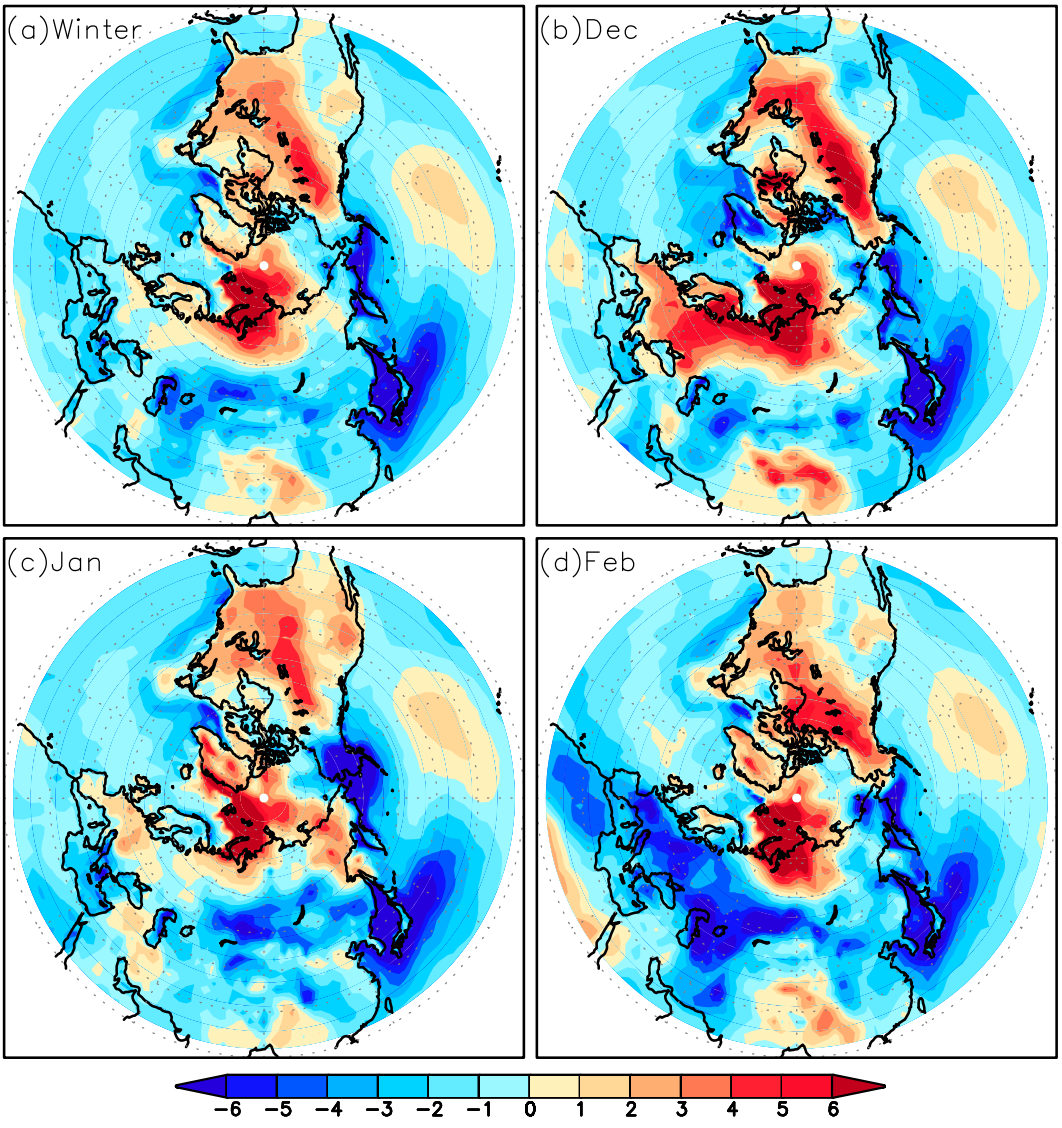

FIG. 14. (a) Observed SAT anomalies (°C) in the winter of 2011/12, relative to the 1979–2012 mean. (b) As in (a), but for December 2011, relative to the 1979–2011 mean. (c) As in (a), but for January 2012, relative to the 1980–2012 mean. (d) As in (c), but for February 2012.

5. Conclusions and discussion

This study investigates dominant features of the atmospheric circulation evolution associated with an extreme cold event in Asia during 17 January–1 February 2012 and its possible association with Arctic sea ice loss. Results highlight the northeastern Pacific–Aleutian region and central Eurasia as two critical precursor areas for the cold event. A steady rise in SLP over the Aleutian region occurred prior to the cold-air outbreak, and then falling SLP over this region coincided with the formation of a polar blocking high aloft coupled with rapid strengthening of the Siberian high, which ushered cold advection over the Asian continent.

Model simulation experiments demonstrate that the combined impacts of both Arctic sea ice loss and atmospheric initial conditions in the summer of 2011 favored the circulation pattern that developed during the ensuing cold winter period, with the initial conditions playing the dominant role. This study also implies that the Aleutian low and disturbances in the midlatitudes over the northeastern Pacific may provide precursors to predict intraseasonal atmospheric evolution over Eurasia.

Although simulation experiments support that the cold event of winter 2011/12 could be largely attributed

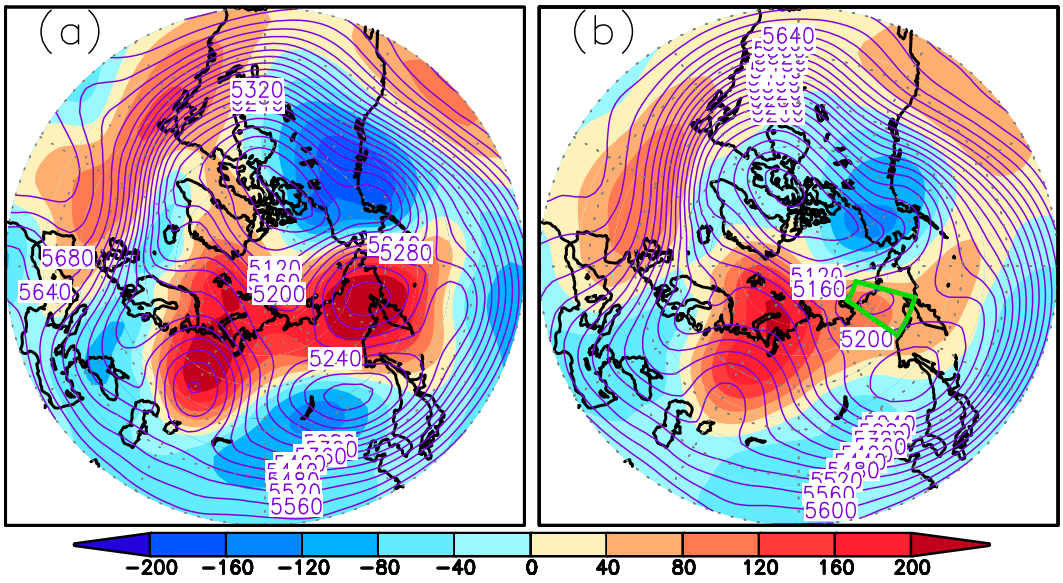

FIG. 15. (a) Contours and shaded areas represent 500-hPa geopotential heights and corresponding anomalies (gpm; relative to the 1979–2012 mean), respectively, averaged over 17–28 Jan 2012. (b) As in (a), but for January 2012. [In (b), the domain 60°–75°N, 145°–165°E surrounded by the green lines is used to calculate the regionally averaged January 500-hPa geopotential heights shown in Fig. 16a.]

to the combined impacts of sea ice loss and atmospheric circulation conditions in the summer of 2011, some questions remain. For example, cold air masses generally move southeastward over Asia, yet observations and simulation experiments exhibited a westward propagation in this case. A possible explanation is that summer atmospheric conditions in the Arctic enhance the feedback of sea ice loss on winter atmospheric variability, which frequently produces a favorable spatial pattern of the mid- and upper-tropospheric steering flow (warm ridges and blocking highs) that promote the occurrence of extremely cold events, leading to a westward propagation of SLP anomalies. Indeed, many details of the mechanism are not yet clear.

A crucial question in understanding this mechanism is how does Arctic sea ice loss affect SLP over the Pacific–Aleutian region and the polar blocking high? Winter Arctic warm anomalies (Fig. 14) precede positive SLP anomalies over the Pacific–Aleutian region and the occurrence of the polar blocking high (Figs. 3 and 4). The spatial patterns of SAT anomalies are similar for the entire winter of 2011/12 and for the three individual winter months, with warm anomalies located mainly over North America, northern Eurasia, Siberian marginal seas, and the Barents–Kara Seas. Positive SAT anomalies for January 2012 closely resemble those averaged over the period of the extremely cold event (Figs. 14c and 2a). Arctic sea ice loss would contribute to Arctic warm anomalies (Screen and Simmonds 2010). The combined impacts of both Arctic sea ice loss and atmospheric circulation conditions in the previous summer season were the primary causes of observed SLP anomalies in the winter of 2011/12 and January 2012, leading to strengthened SLP over the Siberia and the northern Pacific region (Figs. 9a,c, 6c, and 2b). This pattern of SLP anomalies over the mid- and high latitudes in the winter of 2011/12 closely resembles an atmospheric circulation anomaly associated with recent Arctic winter warm anomalies and sea ice loss (Wu 2017). The intensity of this atmospheric circulation anomaly reached the maximum in both of the winter of 2011/12 and January 2012 over the period from 1979 to 2016 (not shown), which was the precondition for positive SLP anomalies over the northern Pacific.

The polar blocking high persisted for 12 days, from 17 to 28 January (Fig. 3). The 500-hPa geopotential heights averaged over this period showed a dual blocking high over the Ural Mountains and far eastern Russia, forming a dumbbell-shaped region of positive height anomalies surrounded by negative height anomalies (Fig. 15a). A similar but weaker spatial pattern was observed in January 2012, including a polar blocking high over far eastern Russia (Fig. 15b). The January regionally averaged 500-hPa geopotential height over the domain bounded by the green box in Fig. 15b is used as an index to characterize the intensity of the polar

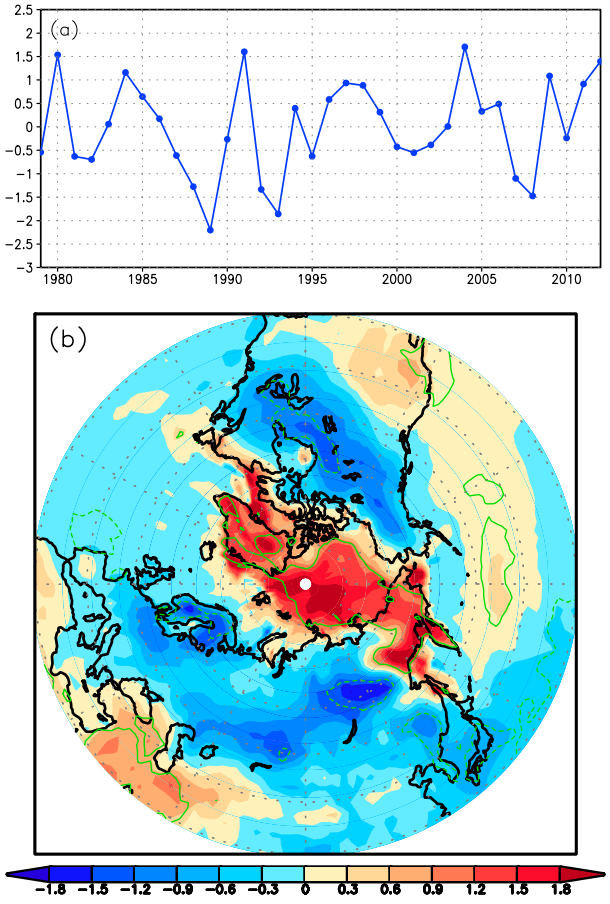

FIG. 16. (a) Normalized time series of January 500-hPa geopotential heights averaged over the domain 60°–75°N, 145°–165°E in Fig. 15b. (b) January SAT anomalies (°C), derived from a linear regression on the normalized time series shown in (a), the green contours indicate SAT anomalies at the 95% significance level.

blocking high. Over the past 34 years, there were only three times that the index exceeded 1.5σ (1980, 1991, and 2004), and it was close to 1.5σ in January 2012 (Fig. 16a). Meanwhile, January positive height anomalies over far eastern Russia correspond to significant positive SAT anomalies over the Arctic and far eastern Russia (Fig. 16b), and both set the stage for the polar blocking high. Consequently, Arctic sea ice loss and Arctic warm SATs are favorable conditions for the occurrence of the polar blocking high, which further strengthens the Siberian high (Takaya and Nakamura 2005b) and triggers cold events. Certainly, the occurrence of the polar blocking high is complicated and influenced by many factors. Many questions remain, such as the exact mechanisms through which Arctic sea ice loss interacts with perhaps prolongs the polar blocking high. These questions will be addressed in future investigations.

We note that if this study instead used the daily SIC forcing, simulation results might differ from those using monthly SIC forcing. The direct impact using daily SICs would likely exhibit larger variability than for monthly SICs, including spatial variability. Because amplitudes of daily SICs are also larger than monthly amplitudes, forcing by daily SICs would tend to amplify daily atmospheric responses. It is unclear, however, if using daily SIC forcing would improve seasonal simulation results over monthly SIC forcing.

Although sea ice loss was substantial in the summer and autumn of 2011, observed and simulated winter atmospheric circulation anomalies consistently exhibited the positive phase of the AO, with predominantly low SLP anomalies over the central Arctic (Figs. 6, 9, and 10). A similar positive phase of the winter AO was also observed in the winter of 2007/08, which followed the second lowest September Arctic sea ice extent on record. Consequently, in contrast to a number of other studies that associate sea ice loss with a tendency for negative AO phases in the ensuing winters, these cases suggest that the association is inconsistent. Clearly further work is needed to understand linkages between increasingly frequent cold winters in Asia and the forcings in months preceding them, as improved long-range prediction of these events is of substantial societal importance.

Acknowledgments. The authors thank three anonymous reviewers for their helpful comments that substantially improved this manuscript. We are grateful to the British Atmospheric Data Centre (BADC) and NCEP–NCAR for providing sea ice concentration data and atmospheric reanalysis data. This study was supported by the National Key Basic Research Project of China (2015CB453200), the National Natural Science Foundation of China (41475080 and 41661144017), and the Basic Research Foundation of CAMS (2015Z001). J.A. Francis was supported by National Science Foundation Grant 1304097.

REFERENCES

Alexander, A., S. Bhatt, and J. Walsh, 2004: The atmospheric response to realistic sea ice anomalies in an AGCM during winter. *J. Climate*, **17**, 890–905, doi:10.1175/1520-0442(2004)017<0890:TARTRA>2.0.CO;2.

Branstator, G., 1987: A striking example of the atmosphere's leading traveling pattern. *J. Atmos. Sci.*, **44**, 2310–2323, doi:10.1175/1520-0469(1987)044<2310:ASEOTA>2.0.CO;2.

Chang, C. P., and K.-M. Lau, 1980: Northeasterly cold surges and near-equatorial disturbances over the winter MONEX area during December 1974. Part II: Planetary-scale aspects. *Mon. Wea. Rev.*, **108**, 298–312, doi:10.1175/1520-0493(1980)108<0298:NCSANE>2.0.CO;2.

——, and ——, 1982: Short-term planetary-scale interaction over the tropics and midlatitudes during northern winter. Part I: Contrasts between active and inactive periods. *Mon. Wea. Rev.*, **110**, 933–946, doi:10.1175/1520-0493(1982)110<0933:STPSIO>2.0.CO;2.

Chen, T.-C., W.-R. Huang, and J.-H. Yoon, 2004: Interannual variation of the east Asian cold surge activity. *J. Climate*, **17**, 401–413, doi:10.1175/1520-0442(2004)017<0401:IVOTEA>2.0.CO;2.

Cohen, J., and Coauthors, 2014: Recent Arctic amplification and extreme mid-latitude weather. *Nat. Geosci.*, **7**, 627–637, doi:10.1038/ngeo2234.

Davies, H. C., 2015: Weather chains during the 2013/2014 winter and their significance for seasonal prediction. *Nat. Geosci.*, **8**, 833–837, doi:10.1038/ngeo2561.

Deser, C., G. Magnusdottir, R. Saravanan, and A. Phillips, 2004: The effects of North Atlantic SST and sea ice anomalies on the winter circulation in CCM3. Part II: Direct and indirect components of the response. *J. Climate*, **17**, 877–889, doi:10.1175/1520-0442(2004)017<0877:TEONAS>2.0.CO;2.

Ding, Y.-H., 1990: Build-up, air mass transformation and propagation of Siberian high and its relation to cold surge in east Asia. *Meteor. Atmos. Phys.*, **44**, 281–292, doi:10.1007/BF01026822.

——, and T. N. Krishnamurti, 1987: Heat budget of Siberian high and winter monsoon. *Mon. Wea. Rev.*, **115**, 2428–2449, doi:10.1175/1520-0493(1987)115<2428:HBOTSH>2.0.CO;2.

Francis, J., and S. Vavrus, 2012: Evidence linking Arctic amplification to extreme weather in mid-latitudes. *Geophys. Res. Lett.*, **39**, L06801, doi:10.1029/2012GL051000.

——, and ——, 2015: Evidence for a wavier jet stream in response to rapid Arctic warming. *Environ. Res. Lett.*, **10**, 014005, doi:10.1088/1748-9326/10/1/014005.

Gong, D.-Y., and C.-H. Ho, 2002: The Siberian high and climate change over middle to high latitude Asia. *Theor. Appl. Climatol.*, **72**, 1–9, doi:10.1007/s007040200008.

Hadley Centre for Climate Prediction and Research, 2006: Met Office HadISST 1.1—Global sea-Ice coverage and Sea Surface Temperature (1870-2015). NCAS British Atmospheric Data Centre, accessed 5 January 2016. [Available online at http://catalogue.ceda.ac.uk/uuid/facafa2ae494597166217a9121a62d3c.]

Honda, M., J. Inous, and S. Yamane, 2009: Influence of low Arctic sea-ice minima on anomalously cold Eurasian winters. *Geophys. Res. Lett.*, **36**, L08707, doi:10.1029/2008GL037079.

Jaiser, R., K. Dethloff, and D. Handorf, 2013: Stratospheric response to Arctic sea ice retreat and associated planetary wave propagation changes. *Tellus*, **65A**, 19375, doi:10.3402/tellusa.v65i0.19375.

Jeong, J.-H., and C.-H. Ho, 2005: Changes in occurrence of cold surges over east Asia in association with Arctic Oscillation. *Geophys. Res. Lett.*, **32**, L14704, doi:10.1029/2005GL023024.

——, B.-M. Kim, C.-H. Ho, D. Chen, and G.-H. Lim, 2006: Stratospheric origin of cold surge occurrence in east Asia. *Geophys. Res. Lett.*, **33**, L14710, doi:10.1029/2006GL026607.

Kug, J., J. Jeong, Y. Jang, B. Kim, C. Folland, S. Min, and S. Son, 2015: Two distinct influences of Arctic warming on cold winters over North America and East Asia. *Nat. Geosci.*, **8**, 759–762, doi:10.1038/ngeo2517.

Kushnir, Y., 1987: Retrograding wintertime low-frequency disturbances over the North Pacific Ocean. *J. Atmos. Sci.*, **44**, 2727–2742, doi:10.1175/1520-0469(1987)044<2727:RWLFDO>2.0.CO;2.

Li, C., B. Stevens, and J. Marotzke, 2015: Eurasian winter cooling in the warming hiatus of 1998–2012. *Geophys. Res. Lett.*, **42**, 8131–8139, doi:10.1002/2015GL065327.

Liu, J., J. Curry, H. Wang, M. Song, and R. Horton, 2012: Impact of declining Arctic sea ice on winter snowfall. *Proc. Natl. Acad. Sci. USA*, **109**, 4074–4079, doi:10.1073/pnas.1114910109.

Magnusdottir, G., C. Deser, and R. Saravanan, 2004: The effects of North Atlantic SST and sea ice anomalies in the winter circulation in CCM3. Part I: Main features and storm track characteristics of the response. *J. Climate*, **17**, 857–876, doi:10.1175/1520-0442(2004)017<0857:TEONAS>2.0.CO;2.

McCusker, K. E., J. C. Fyfe, and M. Sigmond, 2016: Twenty-five winters of unexpected Eurasian cooling unlikely due to Arctic sea-ice loss. *Nat. Geosci.*, **9**, 838–842, doi:10.1038/ngeo2820.

Meehl, G. A., R. Lukas, G. N. Kiladis, K. M. Weickmann, A. J. Matthews, and M. Wheeler, 2001: A conceptual framework for time and space scale interactions in the climate system. *Climate Dyn.*, **17**, 753–775, doi:10.1007/s003820000143.

Meleshko, V., O. M. Johannessen, A. V. Baidin, T. V. Pavlova, and V. A. Govorkova, 2016: Arctic amplification: Does it impact the polar jet stream? *Tellus*, **68A**, 32330, doi:10.3402/tellusa.v68.32330.

Mori, M., M. Watanabe, H. Shiogama, J. Inoue, and M. Kimoto, 2014: Robust Arctic sea-ice influence on the frequent Eurasian cold winters in past decades. *Nat. Geosci.*, **7**, 869–873, doi:10.1038/ngeo2277.

Nakamura, T., K. Yamazaki, K. Iwamoto, M. Honda, Y. Miyoshi, Y. Ogawa, and J. Ukita, 2015: A negative phase shift of the winter AO/NAO due to the recent Arctic sea-ice reduction in late autumn. *J. Geophys. Res. Atmos.*, **120**, 3209–3227, doi:10.1002/2014JD022848.

Ogi, M., K. Yamazaki, and J. Wallace, 2010: Influence of winter and summer surface wind anomalies on summer Arctic sea ice extent. *Geophys. Res. Lett.*, **37**, L07701, doi:10.1029/2009GL042356.

Overland, J., J. Francis, E. Hanna, and M. Wang, 2012: The recent shift in early summer Arctic atmospheric circulation. *Geophys. Res. Lett.*, **39**, L19804, doi:10.1029/2012GL053268.

——, ——, R. Hall, E. Hanna, S. Kim, and T. Vihma, 2015: The melting Arctic and midlatitude weather patterns: Are they connected? *J. Climate*, **28**, 7917–7932, doi:10.1175/JCLI-D-14-00822.1.

Park, T.-W., J.-H. Jeong, C.-H. Ho, and S.-J. Kim, 2008: Characteristics of atmospheric circulation associated with cold surge occurrences in east Asia: A case study during 2005/06 winter. *Adv. Atmos. Sci.*, **25**, 791–804, doi:10.1007/s00376-008-0791-0.

——, C.-H. Ho, and S. Yang, 2011: Relationship between the Arctic Oscillation and cold surges over East Asia. *J. Climate*, **24**, 68–83, doi:10.1175/2010JCLI3529.1.

Perlwitz, J., M. Hoerling, and R. Dole, 2015: Arctic tropospheric warming: Causes and linkages to lower latitudes. *J. Climate*, **28**, 2154–2167, doi:10.1175/JCLI-D-14-00095.1.

Petoukhov, V., and V. Semenov, 2010: A link between reduced Barents-Kara sea ice and cold winter extremes over northern continents. *J. Geophys. Res.*, **115**, D21111, doi:10.1029/2009JD013568.

Roeckner, E., and Coauthors, 2003: The atmospheric general circulation model ECHAM5. Part I: Model description. Max Planck Institute for Meteorology Rep. 349, 127 pp. [Available online at http://www.mpimet.mpg.de/fileadmin/models/echam/mpi_report_349.pdf.]

Screen, J. A., and I. Simmonds, 2010: The central role of diminishing sea ice in recent Arctic temperature amplification. *Nature*, **464**, 1334–1337, doi:10.1038/nature09051.

——, and ——, 2013a: Exploring links between Arctic amplification and mid-latitude weather. *Geophys. Res. Lett.*, **40**, 959–964, doi:10.1002/grl.50174.

——, and ——, 2013b: Caution needed when linking weather extremes to amplified planetary waves. *Proc. Natl. Acad. Sci. USA*, **110**, E2327, doi:10.1073/pnas.1304867110.

——, C. Deser, I. Simmonds, and R. Tomas, 2014: Atmospheric impacts of Arctic sea-ice loss, 1979–2009: Separating forced change from atmospheric internal variability. *Climate Dyn.*, **43**, 333–344, doi:10.1007/s00382-013-1830-9.

Song, L., L. Wang, W. Chen, and Y. Zhang, 2016: Intraseasonal variation of the strength of the East Asian trough and its climatic impacts in boreal winter. *J. Climate*, **29**, 2557–2577, doi:10.1175/JCLI-D-14-00834.1.

Spreen, G., R. Kwok, and D. Menemenlis, 2011: Trend in Arctic sea ice drift and role of wind forcing: 1992–2009. *Geophys. Res. Lett.*, **38**, L19501, doi:10.1029/2011GL048970.

Takaya, K., and H. Nakamura, 2001: A formulation of a phase-independent wave-activity flux for stationary and migratory quasigeostrophic eddies on a zonally varying basic flow. *J. Atmos. Sci.*, **58**, 608–627, doi:10.1175/1520-0469(2001)058<0608:AFOAPI>2.0.CO;2.

——, and ——, 2005a: Mechanisms of intraseasonal amplification of the cold Siberian high. *J. Atmos. Sci.*, **62**, 4423–4440, doi:10.1175/JAS3629.1.

——, and ——, 2005b: Geographical dependence of upper-level blocking formation associated with intraseasonal amplification of the Siberian high. *J. Atmos. Sci.*, **62**, 4441–4449, doi:10.1175/JAS3628.1.

Tang, Q., X. Zhang, X. Yang, and J. Francis, 2013: Cold winter extremes in northern continents linked to Arctic sea ice loss. *Environ. Res. Lett.*, **8**, 014036, doi:10.1088/1748-9326/8/1/014036.

Van Oldenborgh, G., R. Haarsma, H. Vries, and M. Allen, 2015: Cold extremes in North America vs. mild weather in Europe: The winter of 2013–14 in the context of a warming world. *Bull. Amer. Meteor. Soc.*, **96**, 707–714, doi:10.1175/BAMS-D-14-00036.1.

Walsh, J., 2014: Intensified warming of the Arctic: Causes and impacts on middle latitudes. *Global Planet. Change*, **117**, 52–63, doi:10.1016/j.gloplacha.2014.03.003.

Wang, L., and W. Chen, 2014: The East Asian winter monsoon: Re-amplification in the mid-2000s. *Chin. Sci. Bull.*, **59**, 430–436, doi:10.1007/s11434-013-0029-0.

WMO Regional Climate Centres, 2012: Cold spell in Europe and Asia in late winter 2011/2012. WMO Regional Climate Centres, 20 pp. [Available online at http://reliefweb.int/sites/reliefweb.int/files/resources/dwd_2012_report.pdf.]

Wu, B., 2017: Winter atmospheric circulation anomaly associated with recent Arctic winter warm anomalies. *J. Climate*, doi:10.1175/JCLI-D-17-0175.1, in press.

——, J. Su, and R. Zhang, 2011: Effects of autumn-winter arctic sea ice on winter Siberian high. *Chin. Sci. Bull.*, **56**, 3220–3228, doi:10.1007/s11434-011-4696-4.

——, J. Overland, and R. D'Arrigo, 2012: Anomalous Arctic surface wind patterns and their impacts on September sea ice minima and trend. *Tellus*, **64**, 18590, doi:10.3402/tellusa.v64i0.18590.

——, D. Handorf, K. Dethloff, A. Rinke, and A. Hu, 2013: Winter weather patterns over northern Eurasia and Arctic sea ice loss. *Mon. Wea. Rev.*, **141**, 3786–3800, doi:10.1175/MWR-D-13-00046.1.

——, J. Su, and R. D'Arrigo, 2015: Patterns of Asian winter climate variability and links to Arctic sea ice. *J. Climate*, **28**, 6841–6858, doi:10.1175/JCLI-D-14-00274.1.

——, K. Yang, and J. Francis, 2016: Summer Arctic dipole wind pattern affects the winter Siberian high. *Int. J. Climatol.*, **36**, 4187–4201, doi:10.1002/joc.4623.

Zhang, J., W. Tian, M. P. Chipperfield, F. Xie, and J. Huang, 2016: Persistent shift of the Arctic polar vortex towards the Eurasian continent in recent decades. *Nat. Climate Change*, **6**, 1094–1099, doi:10.1038/nclimate3136.

Zhang, Y., and W.-C. Wang, 1997: Model-simulated northern winter cyclone and anticyclone activity under a greenhouse warming scenario. *J. Climate*, **10**, 1616–1634, doi:10.1175/1520-0442(1997)010<1616:MSNWCA>2.0.CO;2.